Scene-based nonuniformity correction using local constant statistics

Chao Zhang[1,*] and Wenyi Zhao[2]

[1]*Sarnoff Corporation, Princeton, New Jersey 08540, USA*
[2]*Present address: Intuitive Surgical Inc., Sunnyvale, California 94086-5304, USA*
[*]*Corresponding author: dzhang@sarnoff.com*

Received October 5, 2007; revised March 29, 2008; accepted March 30, 2008;
posted April 21, 2008 (Doc. ID 88249); published May 29, 2008

In scene-based nonuniformity correction, the statistical approach assumes all possible values of the true-scene pixel are seen at each pixel location. This global-constant-statistics assumption does not distinguish fixed pattern noise from spatial variations in the average image. This often causes the "ghosting" artifacts in the corrected images since the existing spatial variations are treated as noises. We introduce a new statistical method to reduce the ghosting artifacts. Our method proposes a local-constant statistics that assumes that the temporal signal distribution is not constant at each pixel but is locally true. This considers statistically a constant distribution in a local region around each pixel but uneven distribution in a larger scale. Under the assumption that the fixed pattern noise concentrates in a higher spatial-frequency domain than the distribution variation, we apply a wavelet method to the gain and offset image of the noise and separate out the pattern noise from the spatial variations in the temporal distribution of the scene. We compare the results to the global-constant-statistics method using a clean sequence with large artificial pattern noises. We also apply the method to a challenging CCD video sequence and a LWIR sequence to show how effective it is in reducing noise and the ghosting artifacts. © 2008 Optical Society of America

OCIS codes: 100.0100, 030.4280.

1. INTRODUCTION

Focal-plane array (FPA) sensors used in visible-light and infrared imaging systems are known to have fixed (or static) pattern noise superimposed on the true image [1,2]. The noise is attributed to the spatial nonuniformity in the photoresponses of the individual detectors in the array. The response is generally characterized by a linear model:

$$z_t(x,y) = g(x,y)s_t(x,y) + b(x,y), \tag{1}$$

where $s_t(x,y)$ is the true signal of a single detector at (x,y) at time t, $g(x,y)$ is the gain, and $b(x,y)$ is the offset. Generally speaking, gain and offset are both a function of time t, as they change slowly along with temperature change.

Two-point nonuniformity correction (NUC) is the most commonly used technique to counteract this noise at startup. The technique requires two distinct sources, e.g., two uniform heat sources in an infrared imaging system [1,3]. Since two distinct sources are hard to maintain, camera manufacturers use one source to counteract the offset drift in a real-time application, which is often referred to as one-point NUC. In one-point NUC, gain information can be stored in a lookup table as a function of temperature and can be loaded on update. The single source calibration corrects the offset. No matter what calibration is used, the static calibration processes need to interrupt the real-time video operations.

Scene-based NUC has been developed to overcome these drawbacks by continuously correcting FPA nonuniformity without reset. There are two main categories of scene-based NUC: Statistical methods [4–6] and registration methods [7–11]. In the statistical methods, a common statistical assumption is to assume that all possible values of the true-scene pixel are seen at each pixel location (from which is derived the name constant-statistics, or global-constant-statistics, as we call it to differentiate from the local-constant statistics of our approach). Based on this assumption, the offset and gain are related to the temporal mean and standard deviation of the pixels at the pixel location. Compared to statistical methods, the registration methods assume that aligned images have the same true-scene pixel at the pixel location.

In general, statistical methods are not computationally expensive and are easy to implement. A problem of using these methods results from the statistical approach requiring many frames and the camera needing to move in such a way as to satisfy the statistical conditions. Registration methods require many fewer frames. However, they rely on accurate global and local motion estimation, and are computationally expensive. The assumption of the same true-scene pixel in the aligned image can be negated when the true signal response is affected by lighting changes, automatic gain control (AGC) of the camera, and random noise.

Both approaches are susceptible to "ghosting" artifacts when a scene remains stationary or the camera freezes [4,12,13]. A simple deghosting method is to detect the changes between frames and deselect the input image if the change is less than a threshold. Another "ghosting" artifact occurs when the global-constant-statistics assumption in the statistical approach is violated, i.e., the range or distribution of possible values of the true-scene

pixels is different at various pixel locations. To understand this problem, we give an example in Fig. 1. Figure 1(a) is a sample image in a video sequence (≈3,700 frames) taken by a visible-light (electro-optic) (EO) camera on a moving vehicle. The camera sees plants, trees, cars; people walking, buildings, etc; the vehicle runs, turns, and pauses. Often the video shows half sky and half ground; thus the average image of the sequence in Fig. 1(b) has a bright-dark-gray area. The available statistical methods would assume a constant mean and thus regard any spatial variation in the average image to be offset. This overshoot will leave a reverse ghost image in the scene. In what follows we will introduce a new statistical method to reduce ghosting artifacts. Our method considers local-constant statistics instead of global-constant statistics to counteract the overshoot.

The rest of the paper is organized as follows. Section 2 reviews the global-constant method and addresses our local-constant method. To separate out the fixed pattern noise from the spatial variations of the average scene, we introduce our spectrum-shaping method using wavelet domain. Section 3 discusses experiments of local- and global-constant-statistics methods applied to an artificial noise sequence, a challenging CCD video sequence, and a long-wave infrared (LWIR) sequence. The conclusion is drawn in Section 4, where we also discuss briefly a more general local-statistics approach that solves gain and offset by the minimization of error functions.

2. LOCAL-CONSTANT-STATISTICS METHOD

In this section, we first review the global-constant-statistics method, and then discuss the local-constant-statistics method, and present the spectrum shaping method. The final subsection focuses on the local-constant algorithm.

A. Review of Global-Constant Statistics

The global-constant-statistics (GCS) algorithms assume that the temporal mean and standard deviation of the true signals at each pixel are constant over space and time. Since zero mean and unity standard deviation of the true signals $s_t(x,y)$ are assumed, the gain and offset at each pixel are related to them in the following equations [4,12]:

$$b(x,y) \cong m(x,y) = \sum_{t=0}^{T-1} \frac{z_t(x,y)}{T}, \tag{2}$$

$$g(x,y) \cong \sigma(x,y) = \sqrt{\frac{\sum_{t=0}^{T-1} [z_t(x,y) - m(x,y)]^2}{T-1}}, \tag{3}$$

where $m(x,y)$ is the temporal mean of the response signals at (x,y), and $\sigma(x,y)$ is the temporal standard deviation at (x,y). T is the number of frames in a sequence. Both mean and deviation can be obtained recursively. The estimated true signal at (x,y) is expressed as

$$\hat{s}_t(x,y) = \frac{z_t(x,y) - b(x,y)}{g(x,y)}. \tag{4}$$

B. Local-Constant Statistics

To develop the local-constant-statistics (LCS) approach, we rewrite the offset and gain in terms of temporal mean $m(x,y)$ and standard deviation $\sigma(x,y)$ and their spatial average of the temporal mean $\langle m \rangle$ and deviation $\langle \sigma \rangle$:

$$g(x,y) = \sigma(x,y) \big/ \langle \sigma \rangle, \tag{5}$$

$$b(x,y) = m(x,y) - g(x,y) m_s(x,y), \tag{6}$$

where m_s is the temporal mean of the true signals. To satisfy the zero-mean offset condition, under GCS, the spatial average $\langle m_s \rangle$ can be obtained in terms of $\langle m \rangle$ and $\langle g \rangle$:

$$\langle m_s \rangle = \frac{\langle m \rangle}{\langle g \rangle}, \quad m_s(x,y) = \langle m_s \rangle. \tag{7}$$

If Eq. (7) is used, Eqs. (5) and (6) can be regarded as general formulas for GCS. However, as we have seen from Fig. 1, when the relations in Eq. (7) no longer hold, we need a new statistical assumption to compute $m_s(x,y)$.

The LCS assumes that the temporal signal distribution is constant locally at each pixel. This assumes statisti-

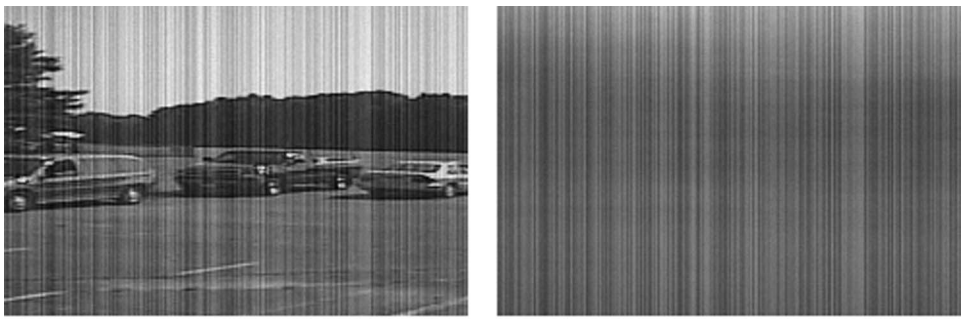

(a) (b)

Fig. 1. (a) Sample image in a video sequence taken by a camera in a moving vehicle. (b) The average image of 2 000 frames in the sequence.

cally constant distribution in a local region around each pixel but uneven distribution in a larger scale. Mathematically, we assume that an equal range and distribution of true-scene signals is seen in a block around each pixel location. This implies

$$F \otimes m_s(x,y) \cong (x,y), \tag{8}$$

where F is a filter or a local operator around (x,y), and $\otimes$ represents the convolution operation. The filter size is determined by the frequency response of the fixed pattern noise and the scene. Furthermore, assume the change of gain is small,

$$F \otimes (gm_s) \cong (F \otimes g)m_s = (F \otimes g)(\langle m_s \rangle + \delta m_s): \tag{9}$$

this leads to a first-order approximation

$$\delta m_s = \frac{F \otimes m}{F \otimes g} - \langle m_s \rangle, \tag{10}$$

and using Eq. (6),

$$b = m - g\langle m_s \rangle - g\,\delta m_s, \tag{11}$$

where δm_s represents the spatial variations caused by the signals in the average image. In Subsection 2.C, we assume b has a much larger spatial variation compared to m_s, i.e., $\delta b \gg \delta m_s$. We will discuss a wavelet method that decomposes the offset image into a Laplacian pyramid and shapes the low frequency image such that it effectively removes δm_s from the offset. Similarly, gain image in Eq. (5) can be rewritten as

$$g(x,y) = \sigma(x,y)/\langle \sigma \rangle - \delta g_s(x,y), \tag{12}$$

where $g_s(x,y)$ represents the variations introduced by the signals. Since $\delta g \gg \delta g_s$, we will apply the spectrum shaping to the gain image to remove the distribution variations from the signals and therefore obtain a better gain estimate.

C. Spectrum Shaping

The spectrum shaping in the wavelet domain on the gain and offset image is addressed here. The general class of linear transform decomposes an image into various components by multiplication with a set of transform functions. Here, we decompose the original image into a Laplacian pyramid [14–16]. The pyramid generation process consists of a low passband G_i and a high passband L_i, where G_i is a subsample of the blurred image of G_{i-1}, and L_i is the difference between G_{i-1} and G_i before G_i is subsampled. We apply a 9×9 normal filter at each level to blur the Gaussian image. Thus, an original image is decomposed into levels of Laplacians and a Gaussian image at the highest level of the pyramid; the reconstruction of the image can be done in a reverse order. Based on the characteristics of the pattern noise with respect to the signal average, we shape the highest level of Gaussian to make it a constant image, and thus reduce the influence of the ghosting artifacts on the noise images. The filter size can be changed. There is no critical difference between a 3×3 filter or a 9×9 filter. However, the maximum decomposition level (n) of the Laplacian pyramid varies accordingly, as it must satisfy the LCS assumption.

1. Spectrum Shaping on Gain

From Subsection 2.B, the gain image is obtained from the ratio of the local standard deviation over the spatial average of the deviation. We rewrite Eq. (12) into a Gaussian image,

$$G_0 = g(x,y) + \delta g_s(x,y) = \sigma(x,y)/\langle \sigma \rangle: \tag{13}$$

G_0 can be decomposed into a multispectral and multiscale representation, or a Laplacian pyramid representation, where each subband of the pyramid contains a certain frequency band of the image:

$$G_0 = L_0 \oplus L_1 \oplus L_2 \oplus \cdots \oplus L_{n-1} \oplus G_n. \tag{14}$$

The Gaussian image at level $i+1$ is obtained from level i by smoothing with a filter F and reducing by half,

$$G_{i+1} = (F \otimes G_i)\downarrow 2, \tag{15}$$

and the Laplacian image at level i is the convolution of $(1-F)$ on the Gaussian image,

$$L_i = (1 - F) \otimes G_i. \tag{16}$$

The Laplacian image at level 0 contains the highest frequency band of the image, and higher levels contain lower-frequency bands. We set G_n to be an identity DC image for all pixels in the image. This spectral shaping operation removes $\delta g_s(x,y)$, the influence of the uneven distribution of signals, from Eq. (13). By summing the subbands, we can reconstruct the Gaussian image G_0 as

$$g \approx G_{est} = L_0 \oplus L_1 \oplus L_2 \oplus \cdots \oplus L_{n-1} \oplus DC. \tag{17}$$

2. Spectrum Shaping on Offset

From Subsection 2.B, we remember that the offset can be obtained from Eq. (11), as the estimate of gain is obtained from Eq. (17). Similar to the gain image, we apply the spectrum-shaping method to obtain b from Eq. (11). After rewriting, Eq. (11) we obtain an image G_0 as

$$G_0 = b + g\,\delta m_s = m - g\langle m_s \rangle. \tag{18}$$

In Eq. (18), assume that b has a much higher spatial frequency, and δm_s has a much lower frequency. G_0 can be decomposed into a multispectral and multiscale representation, or a Laplacian pyramid representation, where each subband of the pyramid contains a certain frequency band of the image:

$$G_0 = L_0 \oplus L_1 \oplus L_2 \oplus \cdots \oplus L_{n-1} \oplus G_n, \tag{19}$$

Similar to the analysis in gain, the Laplacian image at level 0 contains the highest frequency band of the image, and higher levels contain lower-frequency bands. The assumption of the spatial variation of b and m_s indicates that b exists in most of the Laplacian subbands, while δm_s is contained mostly in G_n. Therefore, we can set G_n to 0. This spectrum-shaping operation removes the δm_s term from Eq. (18). By summing the subbands, we can reconstruct the Gaussian image G_0 as

$$b \approx G_{est} = L_0 \oplus L_1 \oplus L_2 \oplus \cdots \oplus L_{n-1} \oplus DC. \tag{20}$$

3. Estimate of the Pyramid Level

The number of pyramid levels determines the scale factor that G_0 is subsampled into, which directly relates to the block size that a LCS holds. If the block size is equal to the image size, then this degenerates to the GCS that assumes a constant for all the pixels. In the scene-based application, when a camera's fixed pattern noise is known, we tend to preset the level of pyramid n and compute the accumulated spatial variations of the average signals along the time. n is set such that all the Laplacian images below the nth level contain most of the noise patterns, and above that, contain most of the signal variations. Subsection 3.A.2 utilizes the energy distribution in the pyramid to illustrate this concept. Statistically, the spatial variations in the average image decrease in time, and a threshold can be set to guarantee the condition under which the spectrum-shaping method can be used. If the block size is set much smaller, multiple iterations of LCS can be applied to the same sequence until significant improvement is achieved.

D. Cascading of Offset and Gain

The gain and offset can be updated by cascading with the reference gain and offset. To discuss this, we first define the reference gain and offset to be (g_I, b_I). If the reference NUC applies to the nth image sequence, then the following equation should hold for this sequence:

$$\frac{z_n(x,y) - b_I}{g_I} = g'_n(x,y)s_n(x,y) + b'_n(x,y), \tag{21}$$

where $g'_n(x,y)$ and $b'_n(x,y)$ are the measures of the nth sequence when reference g_I and b_I are given. The estimated gain and offset that apply to the original response signals can be calculated by the following equations:

$$\hat{g}_n(x,y) = g'_n(x,y)g_I(x,y), \tag{22}$$

$$\hat{b}_n(x,y) = g_I(x,y)b'_n(x,y) + b_I(x,y). \tag{23}$$

(g_I, b_I) can be obtained by a two-point calibration or from a scene-based NUC, or simply set to identity if not calibrated. $[\hat{g}(x,y), \hat{b}(x,y)]$ in Eqs. (22) and (23) reflects the noise drift from the initial calibration in sequence n, and is used to update the display for the sequence at $n+1$. If $[\hat{g}(x,y), \hat{b}(x,y)]$ does not drift away from (g_I, b_I), i.e., $\alpha\|\hat{g} - g_I\| + \|\hat{b} - b_I\| < \varepsilon$, (g_I, b_I) is still used as the reference gain and offset to accumulate the statistics for the next sequence; otherwise (g_I, b_I) is updated and the new pair $[\hat{g}(x,y), \hat{b}(x,y)]$is regarded as the reference NUC coefficients for the new sequence.

E. Local-Constant-Statistics Algorithm

The LCS algorithm is described as follows. Given a sequence of input images $I_n^0, I_n^1, I_n^2, \ldots I_n^t, \ldots I_n^{T-2}, I_n^{T-1}$, and a pair of initial reference NUC coefficients g_I, b_I, each image in the sequence of length T is initially corrected by the coefficients. The updated input images are defined as $\{Z_n^t\}$. The temporal mean and standard deviation at each pixel are accumulated, respectively, by the following recursive formula:

$$m_t(x,y) = \begin{cases} Z_n^0 & t = 0 \\ \dfrac{Z_n^t + tm_{t-1}(x,y)}{t+1} & 0 < t < T, \end{cases} \tag{24}$$

$$\sigma_t(x,y) = \begin{cases} Z_n^0 & t = 0 \\ \sqrt{\dfrac{\mathrm{sum}(Z_n^t Z_n^t) - (t+1)m_t(x,y)m_t(x,y)}{t}} & 0 < t < T, \end{cases} \tag{25}$$

where $\mathrm{sum}(Z_n^t Z_n^t) = \mathrm{sum}(Z_n^{t-1} Z_n^{t-1}) + Z_n^t Z_n^t$, $t > 0$.

To reduce the ghosting effect caused by the static scene, a simple static scene exclusion function is used. We check the summation of the absolute difference (SAD) between two consecutive images and exclude those that have little change from their previous image. Once the accumulation is finished, Eqs. (13) and (18) are calculated. The obtained Gaussian images are then used for spectrum shaping to get a better estimate of both gain and offset. Since the gain and offset are computed in terms of the updated image sequence, they need to be cascaded so that they can be applied to the original images. The gain and offset image may need normalization to ensure unity gain and zero-mean offset conditions. Figure 2 shows the flow diagram of the LCS algorithm. The updated gain and offset are used to update the input of the next sequence for display.

3. RESULTS AND DISCUSSION

We apply the LCS method to three examples: One artificial pattern example to compare results with the GCS method based on the ground truth, one challenging CCD video example that demonstrates the effectiveness of the new method that reduces the noise and ghosting artifacts, and an example that shows the application to an uncooled LWIR that has had the most fixed pattern noise problems.

A. Example with Artificial Fixed Pattern Noises

1. Comparative Study of LCS and GCS Methods

The fixed pattern noises were generated from a gain (horizontal 1±5%, vertical ±1%) and offset image (horizontal ±20, vertical ±5) as applied to the gray scale visible-light (EO) sequence shown in Fig. 1. This parking lot video (240×160) is a byte sequence taken by a camera on a moving vehicle. We used 3,700 frames as a sequence and applied LCS for three iterations to make the initial gain and offset computation (the actual number of frames used

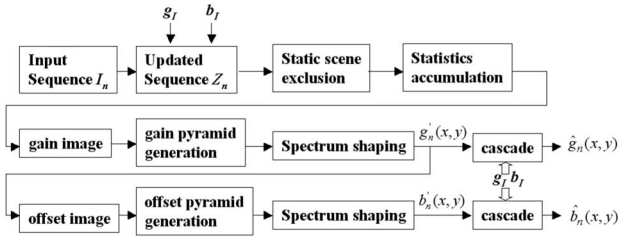

Fig. 2. Diagram of the local-constant-statistics algorithm.

Table 1. RMSE of Gain and Offset Image from GCS and LCS for the Parking Lot Sequence

Parameter	GCS	LCS
Gain	0.22	0.04
Offset	24.49	8.31

in the statistical accumulation was less than that due to the static scene exclusion). The maximum pyramid level was set to four. We use the root of the mean-square-error (RMSE) between the computed pattern image and the original pattern to show the improvement:

$$RMSE(g) = \sqrt{\sum_{i,j} [g(i,j) - g(i,j)]^2/N}, \quad (26)$$

$$RMSE(d) = \sqrt{\sum_{i,j} [\hat{d}(i,j) - d(i,j)]^2/N}, \quad (27)$$

where N is the total number of pixels in the image. The smaller the *RMSE* value, the closer the estimated signals are to the true signals. The *RMSE* of the gain and offset from both GCS and LCS methods are listed in Table 1. It is obvious from the table that the error of the calibration coefficients from the LCS method is reduced significantly compared to the GCS method.

Figure 3 illustrates the difference of gain and offset images obtained from the LCS and GCS methods. Figure 3(a) and 3(b) are the true gain and offset. Figure 3(c) plots the gain on the solid line in Fig. 3(a) from three sources. The curve of circles represents the gain obtained by the LCS method, the curve of squares by GCS method, and the solid curve in the middle is the ground-truth artificial data. The LCS gain is much closer to the ground-truth data than the gain according to GCS. Figure 3(d) plots the offset on the solid line in Fig. 3(b) from the three sources. The LCS offset is closer to the artificial data except for a few points on the left side of the plot.

Figure 4(a) shows the temporal average image after the correction by the LCS method. The pattern noise is superimposed on the average of the true signals as shown in Fig. 1(b). If GCS is used, then the average image should become a constant since the signal mean is assumed to be a constant in the image. To illustrate that the fixed pattern noise is removed while the uneven distribution of the

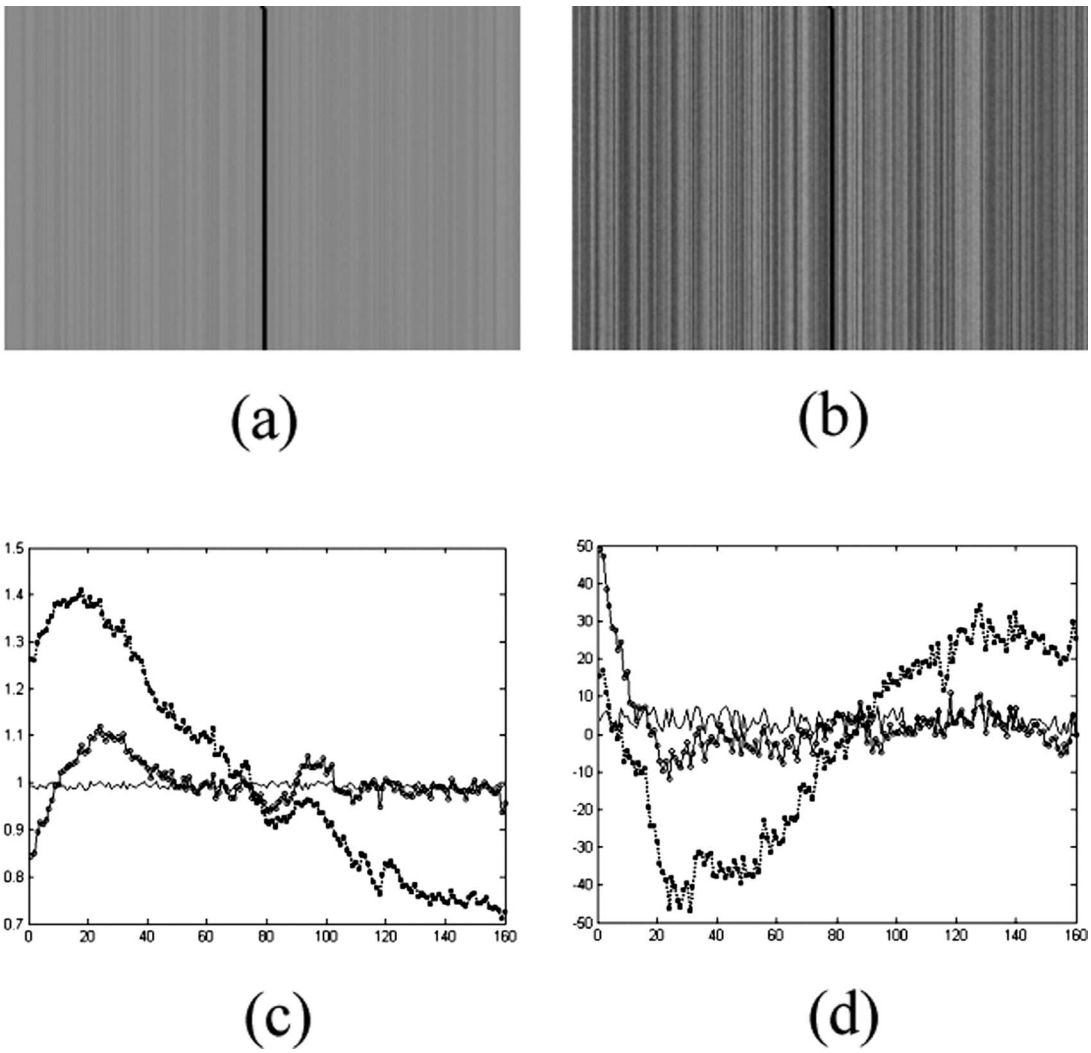

Fig. 3. (a) Original gain, scaled by 128 for display. (b) Original offset, scaled by 2 and offset by 128 for display. The vertical line is used for gain and offset plot. (c) Gain from original, LCS, and GCS. (d) Offset from original, LCS, and GCS.

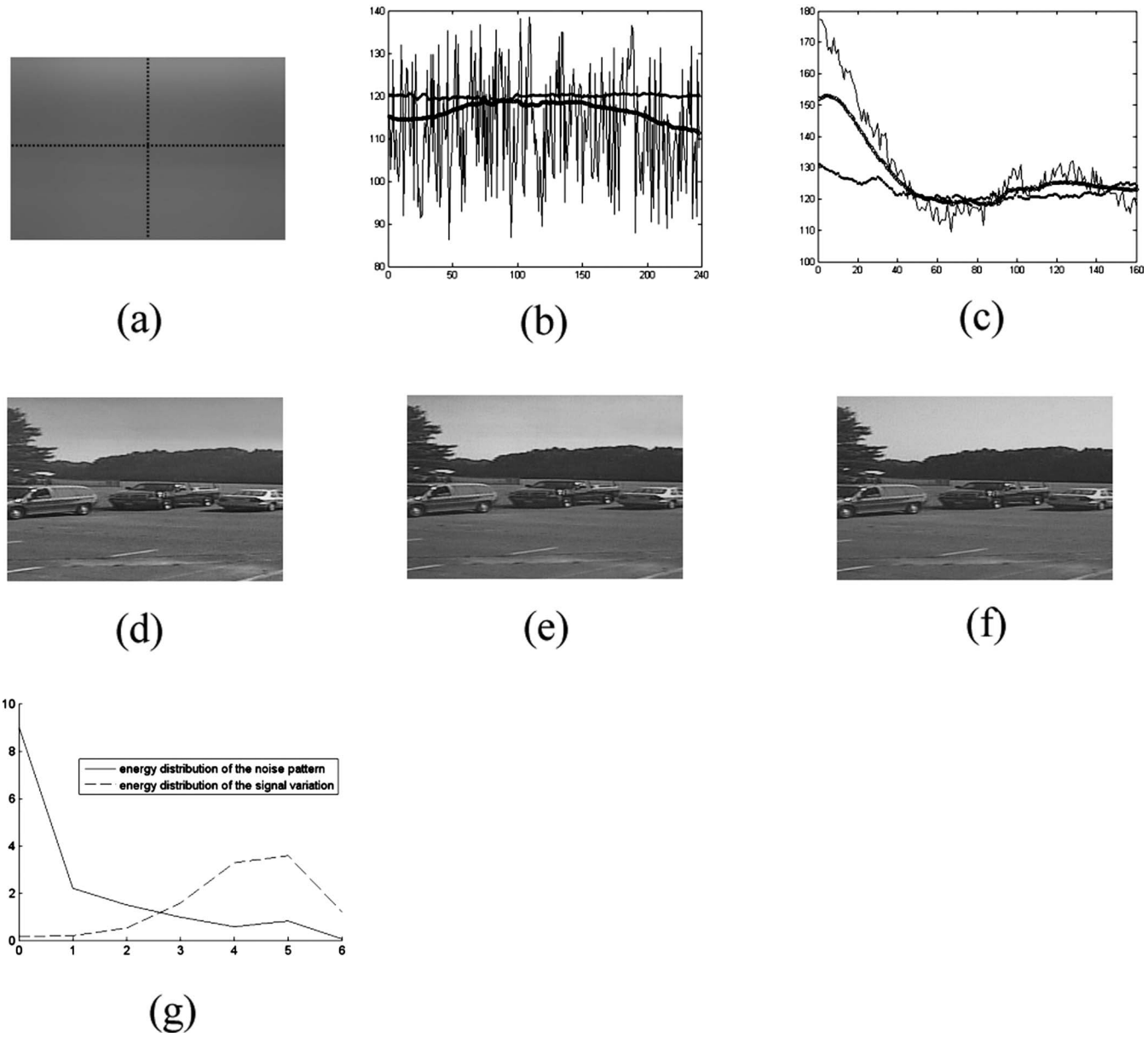

Fig. 4. (a) Temporal average after correction. (b) Plot of values on the dotted horizontal line from the three sources. The jagged solid curve represents the average of the original sequence, circles (top horizontal curve) the average of the corrected sequence using LCS method, squares (bottom horizontal curve) the average using GCS method. (c) Plot of values on the dotted vertical line in (a) from the three sources. The solid curve represents the average of the original sequence, circles the average of the corrected sequence using LCS method, squares the average using GCS method. (d) Nonuniformity corrected image of Fig. 1 in the parking lot sequence using GCS method. (e) Nonuniformity corrected image of Fig. 1 in the parking lot sequence using LCS method. (f) True-scene image. (g) Energy distribution of the noise pattern and the temporal average of the true images in terms of the pyramid levels.

temporal average of the signals is kept in LCS, we pick a horizontal central line and a vertical central line from Fig. 4(a) and plot the gray levels on those two lines. The solid light curve in Fig. 4(b) shows the high oscillatory fixed pattern noise from the original average (on the horizontal line), whose smoothed curve closely matches the curve of circles that represents the LCS result. The GCS average is almost flat.

Figure 4(c) shows the same feature on the vertical line. Even though the ghosting artifacts are not totally removed, they are greatly reduced. This can be verified from Figs. 4(d)–4(f). Figure 4(d) is the nonuniformity corrected result using the GCS method. The sky is distorted by the ghost image and becomes darker. However, we can barely tell the difference between the LCS-corrected image in Fig. 4(e) and the true image in Fig. 4(f). There is no image enhancement applied to the results images. The RMSE of the LCS-corrected image with respect to the true image is $\approx$1.9, and the error of the GCS-corrected image is $\approx$6.6.

2. Comparative Study of the Energy Distribution

We have used the spectral energy distribution in the fixed pattern noise and in the spatial variations of the average image to estimate the maximum pyramid level. The energy at each level is simply computed as the average of the nonzero absolute values in that image. Figure 4(g)

shows the energy distribution of the noise pattern and that of the average image of the true signals with spatial variations. The energy of the noise pattern is distributed mainly in the pyramid level from 0 to 3, while that of the average image has most of the contributions from level 4 and higher. Therefore, we choose to apply the spectrum shaping on the Gaussian image at level 4. For cascaded correction, when most of the noises are corrected from the previous sequence, level 1 can be used as the maximum pyramid level to remove most of the spatial variations in order to update temporal noises.

We have applied a similar analysis to the gain and offset image and obtained the same level results for this sequence. However, since the fixed pattern noise is very different from camera to camera, the pyramid level used in spectrum shaping on the respective gain and offset image is likely different. In another example, the pyramid level for the gain image was 0, with 1 for the offset image. To estimate the gain and offset for a camera in a real application, we suggest that a two-point, or at least a one-point static calibration be performed as a precalibration step. The gain and offset images from the precalibration can be regarded as the ground truth. By applying the energy analysis in the gain and offset pyramid images we can determine the maximum pyramid levels that are used in spectrum shaping for respective gain and offset. In some

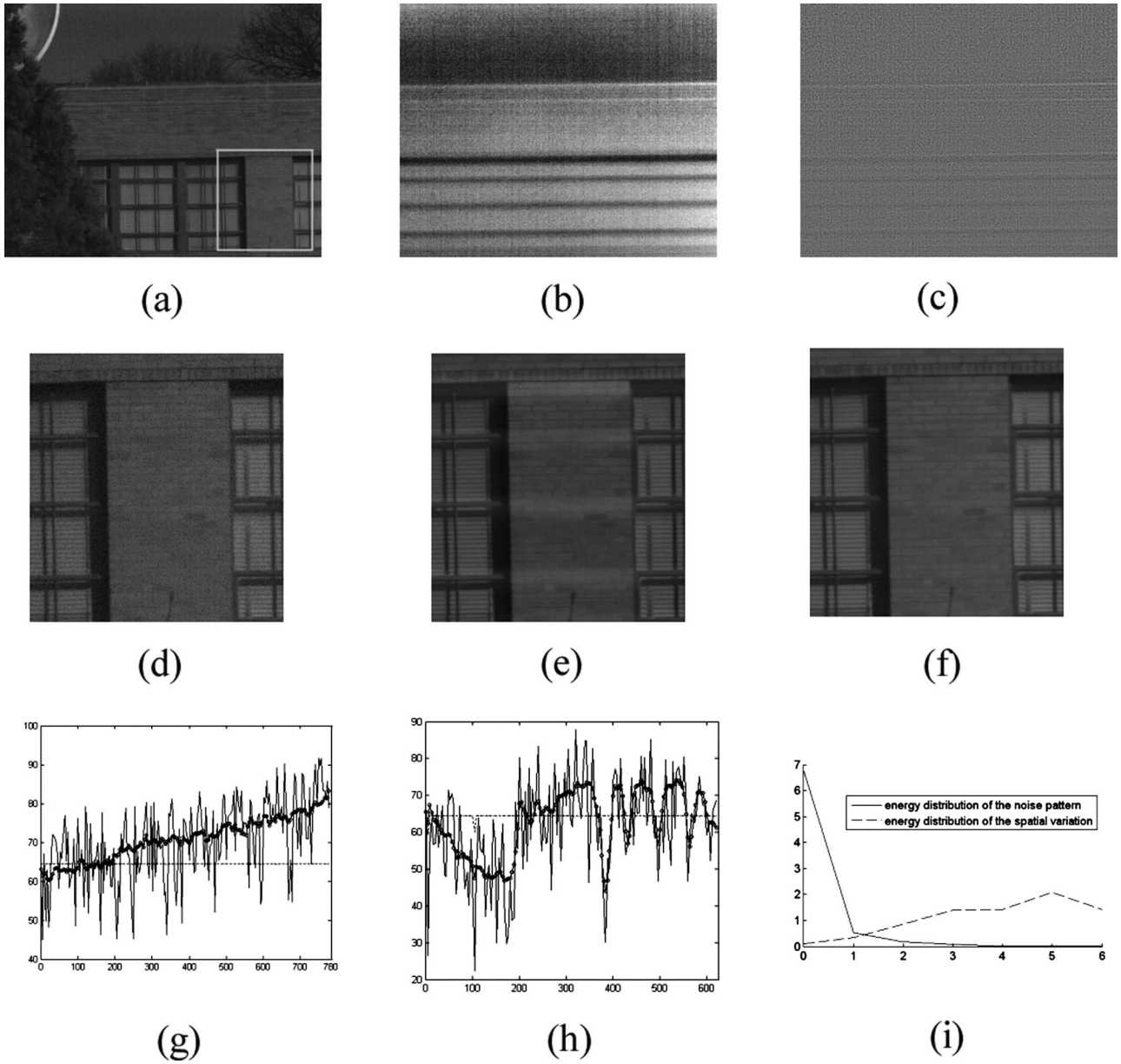

Fig. 5. (a) Sample image from the live sequence. (b) Offset image using GCS method, scaled by 4 and offset by 128. (c) Offset image using LCS method. Maximum pyramid level is set to 1 in spectrum shaping. (d) ROI image from (a). (e) Corrected ROI image using GCS method showing ghosting artifacts. (f) Corrected ROI image using LCS method. (g) Plot of values on the horizontal middle line from the three sources. Solid curve represents the average of the original sequence; circles the average of the corrected sequence using LCS method; squares the average using GCS method. (h) Plot of values on the vertical middle line from the three sources. Solid curve represents the average of the original sequence; circles the average of the corrected sequence using LCS method; squares the average using GCS method. (i) Energy distribution of the noise pattern and the temporal average of the true images in terms of the pyramid levels.

extreme cases, if the spatial energy distribution in each pyramid image is very different, a mask can be defined to allow multiple spatial-related levels being used in spectrum shaping.

The energy distribution plot [Fig. 4(g)] also shows why the LCS method works better than the GCS method. The LCS method works on the level that separates the pattern noise from the spatial variations of the average true signals. As discussed in Subsection 2.C.3, the level is directly related to the block size that satisfies the LCS. However, in the GCS method, since a constant average of the true signals is assumed, it is as if a Gaussian image with single pixel were used at a high level; therefore, all the spatial variations are counted as the pattern noise, and thus cause noticeable ghosting artifacts.

It is also worth mentioning that the Laplacian is a second-order derivative operator; the gradient change is not reflected in the Laplacian energy computation but is maintained in the Gaussian image at the maximum level. This is another advantage of the LCS method: The spectrum shaping of the Gaussian image will definitely remove the influence of the first-order change of the spatial variation from the true signal averages. This also indicates that if the fixed pattern noise contains only first-order gradient changes, the LCS method would not work well.

B. Live Sequence with Fixed Pattern Noises

In this Subsection, we discuss the application of the LCS method to a live sequence. The video sequence is captured from a CCD camera at 250 Hz (780×624 in size, 500 frames). Since the exposure time is very short, the fixed pattern noise is seen on each individual image. In this sequence (see Fig. 5), the camera pans to the right; therefore, the horizontal edge of the building and the window bars become significant features in the average image. For simplicity, and also because of the noise characteristics of the CCD camera, we have assumed unity gain and provide only offset correction to the video sequence. Figure 5(a) is the sample image of the video sequence, and Fig. 5(b) is the offset image using the GCS method. The edges are computed as noises in GCS. When the image is corrected by the offset image, the ghosting artifacts remain in the image, which is enlarged from the region of interest (ROI) in Fig. 5(e) to show that the wall appears to have white strips.

The ghosting artifacts are greatly reduced using the LCS method. The offset image obtained from LCS is in Fig. 5(c) using pyramid level 1 in spectrum shaping based on the measure that most of the noises are in the Laplacian image at level 0 as shown in Fig. 5(i). The corrected image is shown in Fig. 5(f). Compared to the original noise image in Fig. 5(d), we can detect hardly any artifacts. Similar to Fig. 4(c) and 4(d) in which we plotted the pixel values along the horizontal and vertical lines to compare the average of the original sequence and corrected sequences using GCS and LCS methods, Figs. 5(g) and 5(h) display the pixels on these two lines for the live sequence. The DC lines (the dotted lines) represent the GCS result, which treats the signal variations as the noises. The curve of circles is the result of the LCS method, which can be regarded as the local average of the original curve (the solid curve). We can see that it is indeed a better solution to reducing the ghosting artifacts from the images while removing the noise.

Figure 6(a) is the top right corner region from the original sample image, and the noise corrected result is shown in Fig. 6(b) using the LCS method.

C. LWIR Sequence with Fixed and Temporal Noises

We have applied the LCS method to a short LWIR sequence (240×240 in size, 100 frames). The LWIR camera was installed on a vehicle and moved horizontally. All of the images have bright sky, clouds, a bright mountain, and a dark field. The sequence has both temporal and fixed pattern noises in the form of vertical lines. The temporal average of the sequence is an image similar to that of Fig. 1(b). Figure 7(a) represents the original image. The GCS-corrected image in Fig. 7(c) shows a dark sky and a ghostly mountain that is half bright and half dark; the

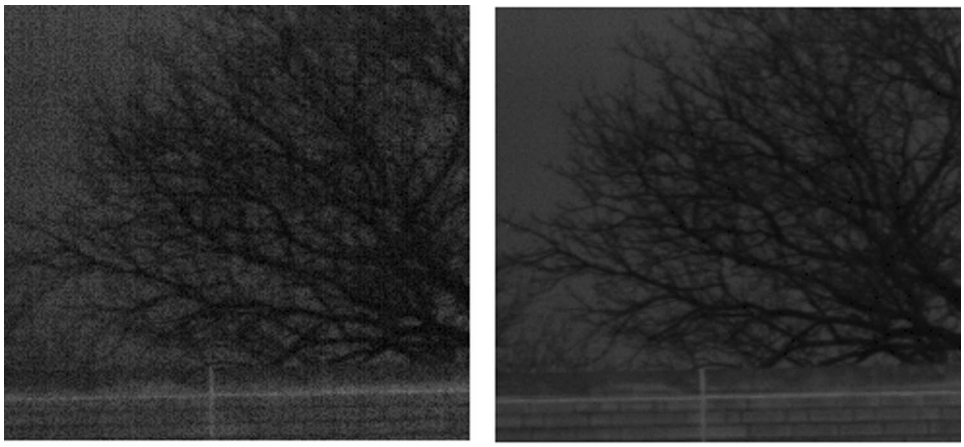

Fig. 6. (a) ROI from the original sample image in Fig. 5(a). (b) Noise-corrected result using LCS method.

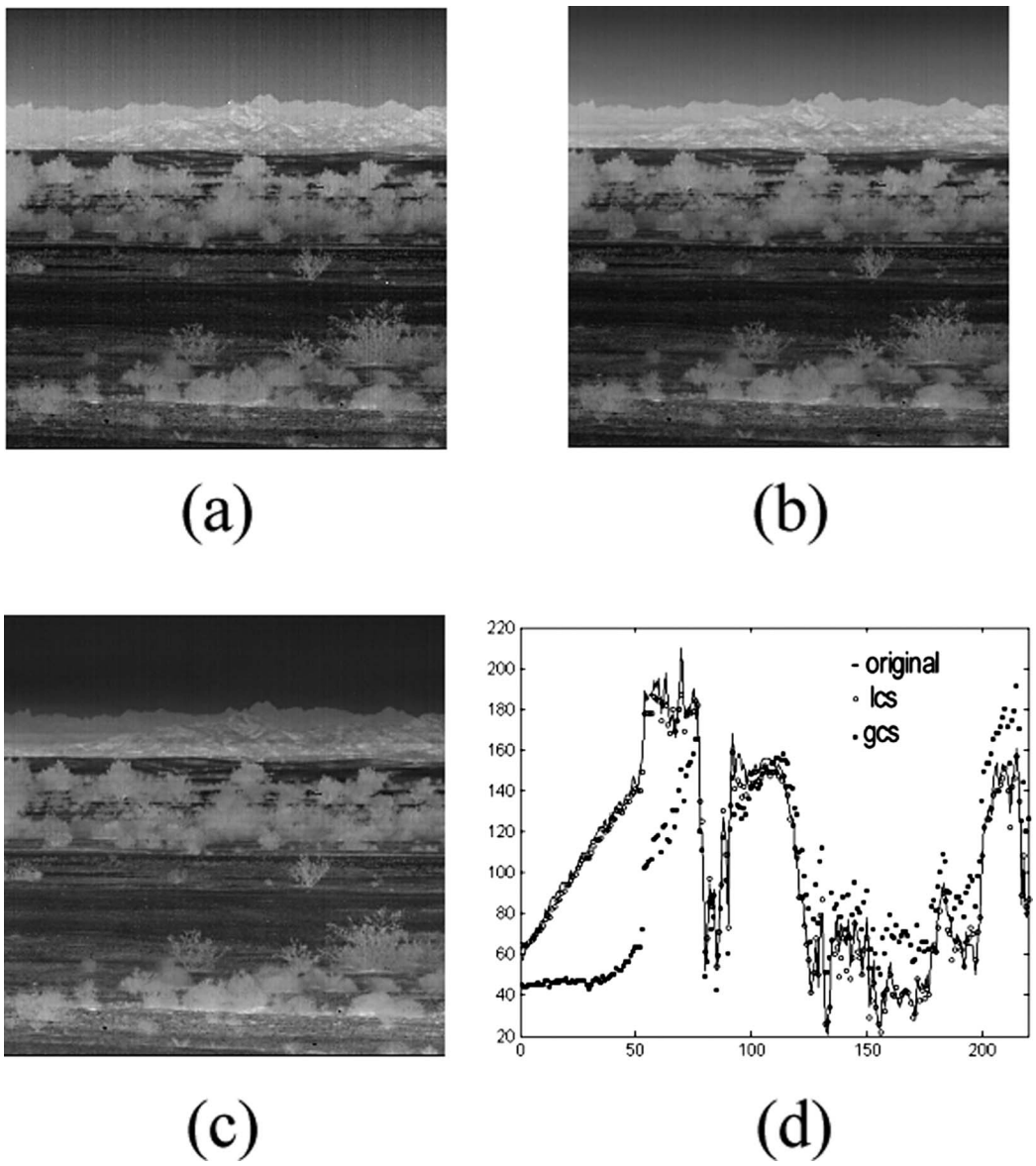

Fig. 7. (a) Sample image from a short LWIR sequence. (b) Corrected LWIR image using LCS method. The maximum pyramid level is set to 1 in spectrum shaping. (c) Corrected LWIR image using GCS method. (d) Plot of the pixel values on the vertical line in the middle of the three sources. Solid curve represents the average of the original sequence, circles the average of the corrected sequence using LCS method, squares, the average using GCS method.

field is much brighter. The LCS-corrected image shown in Fig. 7(b) is much closer to the original image in Fig. 7(a) and has many fewer artifacts. Both GCS- and LCS-corrected images have noticeable fixed pattern noise remaining due to temporally interfering noise.

The pixel values on the vertical line in the middle of the images from the original and the LCS- and GCS-corrected images are plotted in Fig. 7(d) for comparison. This example has demonstrated that the LCS method is able to reduce most of the fixed pattern noise in the presence of other temporal noise, and it reduces the ghosting artifacts that normally result in the GCS method.

4. CONCLUSION AND FUTURE WORK

We have presented a statistical method for nonuniformity correction of the fixed pattern noise in videos. The method adopts a local-constant statistics to estimate gain and offset using a linear model. To remove the fixed pattern noise while maintaining the disparate distribution of the signals, we have used spectrum shaping in the wavelet domain. The proposed algorithm has shown its superiority to global-constant statistics in that it greatly reduces ghosting artifacts that have been introduced in the GCS algorithm. With the selection of different filter size and pyramid level, LCS can work on various ranges of fixed pattern noises. The algorithm can be easily implemented in hardware for real-time application.

A question arises whether the noise reduction technique applied in this paper can be replaced by an image processing function that reduces low spatial information over gain and offset and that can be used directly to improve the GCS method? The answer is probably yes. A

high-pass filtering function with proper filter size can improve the GCS method. However, in Section 3.A.2, we have shown that the energy distribution in different pyramid levels determines the block size of the LCS; if we convert this to the filter size to be used in the high-pass filtering, we are very close to the LCS method.

The theme of this paper is to propose the LCS approach. The approach can be implemented by methods other than spectrum shaping in gain and offset. For example, the histogram of a pixel is a function of the gain and offset, and, given LCS, the gain and offset from its neighbor are related to the center pixel by a translational value b_c and a scale value g_c from the 1D histogram. This can be modeled as a graph with $[g(i,j),b(i,j)]$ as a vertex and (g_c,b_c) as edge. The gain and offset can be generally obtained from the minimization of the two error equations

$$\{g\} = \arg_g \min \sum_{i,j} \sum_{i',j'} [g(i,j) - g_c(i',j' \to i,j) g(i',j')]^2, \tag{28}$$

$$\{b\} = \arg_b \min \sum_{i,j} \sum_{i',j'} [b(i,j) - g_c(i',j' \to i,j) b(i',j') - b_c(i',j' \to i,j)]^2, \tag{29}$$

where (i',j') are defined as the nearest neighbors of (i,j). The summation has been arranged such that there is only one correspondence $(i,j \to i',j')$ or $(i'j' \to i,j)$ in the error functions. The number of (i', j') around (i, j) is determined by the block size that the LCS holds. When extra constraints are provided, the above equations can be solved with least-squares solutions. The details of this method will be discussed in another paper.

As we have learned from the noise images, the LCS method can be used to obtain the "fingerprints" of cameras with the same type of sensors, or even those of a specific camera. The technology could see applications in homeland security, law enforcement, and military services. Because the statistical methods assume the randomness of the true signals, this technology can also be used to detect weak fixed features arising in high random noise.

REFERENCES

1. A. F. Milton, F. R. Barone, and M. R. Kruer, "Influence of nonuniformity on infrared focal plane array performance," Opt. Eng. (Bellingham) **24**, 855–862 (1985).
2. G. C. Holst, *CCD Arrays, Cameras, and Displays* (SPIE Optical Engineering Press, 1996).
3. M. Schulz and L. Caldwell, "Nonuniformity correction and correctability of infrared plane arrays," Infrared Phys. Technol. **36**, 763–777 (1995).
4. J. G. Harris and Y. M. Chiang, "Nonuniformity correction using constant-statistics constraint: Analog and digital implementations," Proc. SPIE **3061**, 895–905 (1997).
5. M. M. Hayat, S. N. Torres, E. E. Armstrong, S. C. Cain, and B. Yasuda, "Statistical algorithm for nonuniformity correction in focal-plane arrays," Appl. Opt. **38**, 772–780 (1999).
6. S. N. Torres and M. M. Hayat, "Kalman filtering for adaptive nonuniformity correction in infrared focal plane arrays," J. Opt. Soc. Am. A **20**, 470–480 (2003).
7. R. C. Hardie, M. M. Hayat, E. E. Armstrong, and B. Yasuda, "Scene-based nonuniformity correction using video sequences and registration," Appl. Opt. **39**, 1241–1250 (2000).
8. B. M. Ratliff, M. M. Hayat, and R. C. Hardie, "Algebraic scene-based nonuniformity correction in focal-plane arrays," Proc. SPIE **4372**, 114–124 (2001).
9. B. M. Ratliff, M. M. Hayat, and R. C. Hardie, "Algebraic algorithm for nonuniformity correction in focal-plane arrays," J. Opt. Soc. Am. A **19**, 1737–1747 (2002).
10. B. M. Ratliff, M. M. Hayat, and J. S. Tyo, "Radiometrically-calibrated scene-based nonuniformity correction for infrared array sensors," Proc. SPIE **4820**, 359–367 (2003).
11. E. E. Armstrong, M. M. Hayat, R. C. Hardie, S. N. Torres, and B. Yasuda, "Nonuniformity correction for improved registration and high-resolution image reconstruction in IR imagery," Proc. SPIE **3808**, 150–161 (1999).
12. J. Harris and Y. M. Chiang, "Minimizing the 'ghosting' artifact in scene-based nonuniformity correction," Proc. SPIE **3377**, 106–112 (1998).
13. R. E. Vera and I. S. Torres, "Ghosting reduction in adaptive non-uniformity correction of infrared focal-plane array image sequences," Proc. IEEE (IEEE, 2003).
14. P. J. Burt, "Fast filter transforms for image processing," Comput. Graph. Image Process. **16**, 20–51 (1981).
15. P. J. Burt and E. H. Adelson, "The Laplacian pyramid as a compact image code," IEEE Trans. Commun. **31**, 532–540 (1983).
16. P. J. Burt and R. J. Kolczynski, "Enhanced image capture through fusion," in *Proceedings of the Fourth International Conference on Computer Vision* (IEEE, 1993), pp. 173–182.